Photon drag in single and multiple two-level quantum wells

Xin Chen and Ole Keller
Institute of Physics, Aalborg University, Pontoppidanstræde 103, DK-9220 Aalborg Øst, Denmark
(Received 21 October 1996; revised manuscript received 21 January 1997)

Starting from a density-matrix operator description we derive an expression for the photon-drag response tensor of a quantum-well system containing an arbitrary number of subbands. Subsequently we analyze the structure of the nonlinear response tensor and make a specialization to the case of a two-level quantum well. In the wake of a self-consistent calculation of the local fields in a two-level well and in multiple quantum wells the photon-drag currents are determined. We illustrate the main ingredients of our theory by carrying out a number of numerical calculations of the drag current in a 15-Å wide niobium quantum well deposited on a crystalline quartz substrate and a $GaAs/Al_xGa_{1-x}As$ multiple-quantum-well structure. In particular we pay attention to the frequency, angle of incidence, and number of wells dependencies of the current, and we demonstrate that local-field effects may give rise to a significant blueshift and an asymmetric form of the resonance peak. [S0163-1829(97)05224-7]

I. INTRODUCTION

In the last decade studies of the photon-drag effect phenomenon in quantum-well structures have attracted some attention, and theoretical[1–5] as well as experimental[6–8] investigations have been carried out. Thus, in the work by Luryi[1] the photon-drag effect accompanying light-induced intersubband transitions in a waveguide formed by an AlAs/GaAs superlattice was studied theoretically, and it was shown that the high intersubband absorption coefficient in combination with the high mobility of the two-dimensional electron gas may lead to a large photon-drag current. The theory of the photon-drag effect in a two-dimensional electron gas system was further developed by Grinberg and Luryi[2] who demonstrated that an enhanced effect may occur due to the difference in the momentum relaxation times in the ground and excited subbands. Particular attention was devoted to the influence of the collision and Doppler shift line broadening in the intersubband absorption. In the work by Stockman *et al.*[3] the light-induced drift of electrons confined in a semiconductor heterostructure was studied and it was shown that the drag current reverses its direction when the electromagnetic frequency is tuned through the relevant electronic transition frequency. This reversal of the current was also found in Ref. 2. In both of the aforementioned works the photon-drag current is antisymmetric with respect to the transition frequency. In the paper by one of the present authors[4] the photon drag effect in a single-level metallic quantum well was studied and the role of local-field effects was examined in detail. The one-level system seems of particular importance for investigations of pure two-dimensional dynamics since electron motions in and out of the well plane are prohibited. In a recent paper by Vasko[5] the photon drag in tunnel-coupled quantum wells was investigated. Readers interested in a recent review and a generalized Boltzmann equation analysis of the photon drag in bulk solids are referred to the paper by Shalaev *et al.*[9] An important experimental study of the resonant photon-drag effect in a GaAs quantum-well system was presented by Wieck *et al.*[6] who showed that the voltage induced by the momentum transfer from the field to the mobile carriers changes sign when the photon frequency is scanned through the electronic resonance. An experimental study aimed at photon-drag detectors for the 10-μm wavelength range was carried out by Kesselring *et al.*[7] Further experimental evidence for the photon-drag phenomenon in two-band metals was given by Shalaev *et al.*[9] who attributed a spatially asymmetry in the photoemission from silver films to the drag effect.

Although a number of important aspects of the drag phenomenon related to intersubband transitions have been investigated in the above-mentioned works,[1–3,5,6] it appears that the local field driving the process has been assumed to be constant across the well. Technically, this means that the interaction Hamiltonian describing the dynamics perpendicular to the plane of the well was approximated by its electric-dipole form. Recent studies of local-field effects in linear and nonlinear optics have shown, however, that particularly in cases where the electron motion perpendicular to the plane of the quantum well is appreciable the prevailing electric field can vary significantly across the well.[10–12] Even in the single-level case local-field effects appear to be of importance.[4]

In the present paper we focus our attention on the role played by local-field effects in cases where intersubband transitions are important for the photon-drag phenomenon. Local-field aspects do not only appear in the calculation of the driving field. Also the nonlinear response function itself exhibits such effects. In the one-level case the photon drag would vanish if local-field effects were neglected in the response function and therefore these effects are indispensable. In the resonant intersubband case it turns out, however, that the relative change of the dominating part of the nonlinear response function is less than $\sim 10^{-3}$ when local-field corrections are involved. Our work therefore shows that only in the driving field itself local-field corrections are needed, but here they are significant. The nonlocal theory of the photon-drag response function given below covers cases where the quantum-well system has many bound states, and only when it comes to the determination of the prevailing field and the

numerical calculation do we specialize ourselves to the two-intersubband case.

Starting from a density-matrix operator approach we derive a general expression for the part of the photon-drag response tensor which is of importance in the present context and we discuss the explicit form of this tensor in the low-temperature limit. Expressions for the photon-drag current density and the drag current itself are also presented in this section. In Sec. II B, the photon drag in a two-level well is calculated. In Sec. III, the theory of the local ac field inside the quantum well is presented and particular emphasis is put on an explicit calculation within the framework of the simple infinite-barrier model. In Sec. IV, the theory is extended to multiple quantum-well structures. The significance of incorporating local-field effects is demonstrated in Sec. V, where a number of numerical results are discussed. Thus, in Sec. V A the quantum-well system we investigate is composed of a niobium quantum well of thickness 15 Å deposited on a crystalline quartz substrate. We have chosen this system because a number of experimental and theoretical investigations of local-field effects in linear and nonlinear optics have already been carried out on this (see, e.g., the review given in Ref. 12). First, the frequency dependence of the nonlinear response function in the vicinity of the intersubband resonance is calculated, and then the frequency and angle of incidence dependencies of the drag current and the local-field corrections to this are determined. We find from these studies that the drag current is blueshifted in frequency and that the resonance exhibits an asymmetric form when local-field effects are taken into account. Finally, we demonstrate that a change in the electric damping rate does not result in any blueshift or (redshift) of the drag resonance. In Sec. V B we investigate the drag current in a $GaAs/Al_xGa_{1-x}As$ multiple quantum-well structure. First, the importance of the radiative coupling among the wells is shown by comparing drag currents calculated with and without radiative interaction among the wells. Next, the frequency dependence of the drag current for different numbers of wells is investigated. Finally, the dependence of the drag current on the number of wells is calculated for three incident photon energies.

II. THEORETICAL FRAMEWORK

A. Photon-drag response tensor and current density

The quantum-well system under consideration consists of a superthin, i.e., a few monolayer thick, metallic film deposited on a dielectric substrate which is characterized by its dielectric constant ε_Q. In a Cartesian xyz-coordinate system the sharp surface of the substrate coincides with the xy plane, and the substrate occupies the half space $z>0$, the boundaries of the quantum well being located at $z=-d$ and $z=0$, as illustrated in Fig. 1. Due to the assumed translational invariance of the quantum-well system parallel to the xy plane, all vector and tensor-field components (T) appearing in our analysis can be expressed in the generic form

$$T(\mathbf{r},t)=T(z)\exp[i(\mathbf{q}_{\|}\cdot\mathbf{r}-\omega t)], \tag{1}$$

where $\mathbf{r}$ and t are the space and time coordinates, respectively, ω denotes the cyclic frequency of the electromagnetic field, and $\mathbf{q}_{\|}$ is the projection of the field wave vector on the xy plane.

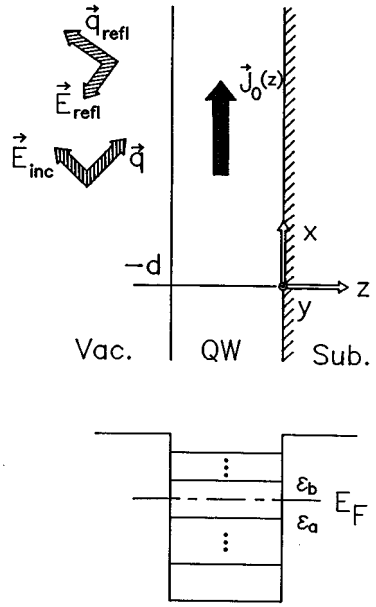

FIG. 1. Upper part: schematic figure showing the metallic quantum-well system under study as well as the Cartesian coordinate system used in the calculation. The thickness of the well is d and a p-polarized incident field $\mathbf{E}_{\rm inc}$ of wave vector $\mathbf{q}$ gives rise to a photon-drag current density $\mathbf{J}_0(z)$ in the quantum well. The ''external'' field which drives the photon-drag phenomenon is composed of the incident field and the field $\mathbf{E}_{\rm refl}$ reflected from the substrate. Lower part: schematic illustration of a quantum well with a square potential. The well is containing a number of bound states and the Fermi energy (E_F) is located between states (a and b) having energies ε_a and ε_b.

In order to investigate the photon-drag effect in the quantum-well system, it is adequate to take as a starting point the following expression for the photon induced nonlinear dc current density:[4]

$$\mathbf{J}_0=\mathrm{Tr}\{\rho^{(0)}_{\rm NL}\mathbf{j}_0\}+\tfrac{1}{4}\mathrm{Tr}\{\rho^{(1)}\mathbf{j}_1^{\dagger}\}+\tfrac{1}{4}\mathrm{Tr}\{(\rho^{(1)})^{\dagger}\mathbf{j}_1\}, \tag{2}$$

where Tr $\{\cdots\}$ denotes the trace of $\{\cdots\}$, $\mathbf{j}_0$ and $\mathbf{j}_1$ are the free and field-perturbed parts of the current density operator, respectively, $\rho^{(1)}$ and $\rho^{(0)}_{\rm NL}$ are the light-induced linear and nonlinear (NL) dc parts of the density-matrix operator, and the dagger stands for Hermitian conjugation. In passing we note that the expression in Eq. (2) is valid to second power in the electric field. Using the relaxation-time approximation, and writing out only the last two terms of Eq. (2), the photon-drag current density is given by

$$\begin{aligned}\mathbf{J}_0=&\,\mathrm{Tr}\{\rho^{(0)}_{\rm NL}\mathbf{j}_0\}\\&+\frac{1}{4}\left[\sum_{M,N}\frac{f_0(E_N)-f_0(E_M)}{\hbar(\omega+i/\tau_{MN})+E_N-E_M}\right.\\&\left.\times\langle M|H^{(1)}|N\rangle\langle N|\mathbf{j}_1^{\dagger}|M\rangle+\text{c.c.}\right],\end{aligned} \tag{3}$$

where $f_0(E)$ is the Fermi-Dirac distribution function, $H^{(1)}$ is the part of the interaction Hamiltonian which is linear in the field, and τ_{MN} is the relaxation time for intersubband transitions between the $|M\rangle$ and $|N\rangle$ energy eigenstates. In this

paper we assume that the relaxation time is the same (τ) for all M and N. For the energy eigenstates single-particle wave functions of the form ($\mathbf{r}$ representation) $\langle \mathbf{r}|M\rangle = (2\pi)^{-1}\exp(i\mathbf{k}_\parallel\cdot\mathbf{r})\psi_m(z)$, etc., are taken, where $\mathbf{k}_\parallel$ is the component of the electron wave vector parallel to the quantum-well surface. By adopting the above-mentioned form it has been assumed the electron motion parallel to the quantum-well plane is free-electron-like. The total energy of the electron in the Mth energy eigenstate thus is given by $E_M=\varepsilon_m+\hbar^2k_\parallel^2/2m_0$, m_0 being the electron mass. Since the first term on the right-hand side of Eq. (3) gives rise to a current density

$$(\overleftrightarrow{\mathbf{U}}-\mathbf{e}_z\mathbf{e}_z)\cdot \mathrm{Tr}\{\rho_{\mathrm{NL}}^{(0)}\mathbf{j}_0\} = \sum_{M,N}\langle N|\rho_{\mathrm{NL}}^{(0)}|M\rangle(\overleftrightarrow{\mathbf{U}}-\mathbf{e}_z\mathbf{e}_z)\cdot\langle M|\mathbf{j}_0|N\rangle, \tag{4}$$

along the quantum well, $\overleftrightarrow{\mathbf{U}}$ being the unit tensor and $\mathbf{e}_z$ a unit vector in the z direction, and since one can show that $(\overleftrightarrow{\mathbf{U}}-\mathbf{e}_z\mathbf{e}_z)\cdot\langle M|\mathbf{j}_0|N\rangle \propto \psi_n(z)\psi_m^*(z)$, the orthogonality of the wave functions of the energy eigenstates implies that the integral of the current density in Eq. (4) over the quantum well vanishes, i.e.,

$$(\overleftrightarrow{\mathbf{U}}-\mathbf{e}_z\mathbf{e}_z)\cdot\int_{-d}^{0}\mathrm{Tr}\{\rho_{\mathrm{NL}}^{(0)}\mathbf{j}_0\}dz=\mathbf{0}. \tag{5}$$

In the following the explicit expression for $\mathrm{Tr}\{\rho_{\mathrm{NL}}^{(0)}\mathbf{j}_0\}$ is not needed.

Let us then consider the situation where the monochromatic plane wave is incident upon the quantum-well system at an angle of incidence $\theta=\arcsin[q_\parallel c_0/(\omega\sqrt{\varepsilon^B})]$. From Eq. (3) one obtains the following z-dependent photon-drag current density:

$$\mathbf{J}_0(z)=\mathrm{Tr}\{\rho_{\mathrm{NL}}^{(0)}\mathbf{j}_0\}+\frac{1}{2}\left[\int\overleftrightarrow{\mathbf{\Pi}}(z,z',z''):\mathbf{E}^*(z')\times\mathbf{E}(z'')dz'dz''+\mathrm{c.c.}\right], \tag{6}$$

where $\mathbf{E}(z)[\equiv\mathbf{E}(z,\mathbf{q}_\parallel,\omega)]$ is the z-dependent amplitude of the local electric field $\mathbf{E}(\mathbf{r},t)=\mathbf{E}(z,\mathbf{q}_\parallel,\omega)\exp[i(\mathbf{q}_\parallel\cdot\mathbf{r}-\omega t)]$. Using real wave functions, the so-called second-order photon-drag response tensor $\overleftrightarrow{\mathbf{\Pi}}(z,z',z'')$ for the quantum-well is given by

$$\overleftrightarrow{\mathbf{\Pi}}(z,z',z'')=\frac{e^2}{2m_0\omega^2}\int\sum_{m,n}\frac{f_0[\varepsilon_n+\hbar^2|\mathbf{k}_\parallel-\mathbf{q}_\parallel|^2/(2m_0)]-f_0[\varepsilon_m+\hbar^2k_\parallel^2/(2m_0)]}{\hbar(\omega+i/\tau)+\varepsilon_n-\varepsilon_m+\hbar^2|\mathbf{k}_\parallel-\mathbf{q}_\parallel|^2/(2m_0)-\hbar^2k_\parallel^2/(2m_0)} \times\delta(z'-z)\psi_m(z)\psi_n(z)\overleftrightarrow{\mathbf{U}}\mathbf{j}_{nm}(\mathbf{k}_\parallel,\mathbf{k}_\parallel-\mathbf{q}_\parallel,z'')\frac{d^2k_\parallel}{(2\pi)^2}, \tag{7}$$

where δ is the Dirac delta function, e is the electron charge, and $\mathbf{j}_{nm}(\mathbf{k}_\parallel,\mathbf{k}_\parallel-\mathbf{q}_\parallel,z'')$ is the transition current density which is given by

$$\mathbf{j}_{nm}(\mathbf{k}_\parallel,\mathbf{k}_\parallel-\mathbf{q}_\parallel,z'')=-\frac{e\hbar}{2im_0}[i(2\mathbf{k}_\parallel-\mathbf{q}_\parallel)\phi_{nm}(z'')+\Phi_{nm}(z'')\mathbf{e}_z], \tag{8}$$

with $\phi_{nm}(z'')=\phi_{mn}(z'')=\psi_n(z'')\psi_m(z'')$ and $\Phi_{nm}(z'')=-\Phi_{mn}(z'')=\psi_n(z'')[d\psi_m(z'')/dz'']-\psi_m(z'')[d\psi_n(z'')/dz'']$. If the electronic damping rate is zero ($\tau\to\infty$) the integrand in Eq. (7) has a pole at $\hbar\omega+\varepsilon_n+\hbar^2|\mathbf{k}_\parallel-\mathbf{q}_\parallel|^2/(2m_0)=\varepsilon_m+\hbar^2k_\parallel^2/(2m_0)$. This relation expresses the energy conservation in a process where an electron is excited by the electromagnetic field from state n to state m, conserving the (pseudo) momentum ($\mathbf{k}_\parallel-\mathbf{q}_\parallel\to\mathbf{k}_\parallel$). To distinguish between the contributions from the various physical processes and to facilitate the calculation of the integrations over the $\mathbf{k}_\parallel$ domain, we rewrite $\overleftrightarrow{\mathbf{\Pi}}(z,z',z'')$ as

$$\begin{aligned}\overleftrightarrow{\mathbf{\Pi}}(z,z',z'')&=\int\sum_{m,n}\{f_0[\varepsilon_n+\hbar^2|\mathbf{k}_\parallel-\mathbf{q}_\parallel|^2/(2m_0)]-f_0[\varepsilon_m+\hbar^2k_\parallel^2/(2m_0)]\}\overleftrightarrow{\mathbf{D}}_{nm}\frac{d^2k_\parallel}{(2\pi)^2}\\ &=\int\Bigg[\sum_{\substack{m,n\\ \varepsilon_m<E_F\\ \varepsilon_n<E_F}}\{f_0[\varepsilon_n+\hbar^2|\mathbf{k}_\parallel-\mathbf{q}_\parallel|^2/(2m_0)]-f_0[\varepsilon_m+\hbar^2k_\parallel^2/(2m_0)]\}+\sum_{\substack{m,n\\ \varepsilon_m<E_F\\ \varepsilon_n>E_F}}\{f_0[\varepsilon_n+\hbar^2|\mathbf{k}_\parallel-\mathbf{q}_\parallel|^2/(2m_0)]\\ &\quad-f_0[\varepsilon_m+\hbar^2k_\parallel^2/(2m_0)]\}+\sum_{\substack{m,n\\ \varepsilon_m>E_F\\ \varepsilon_n<E_F}}\{f_0[\varepsilon_n+\hbar^2|\mathbf{k}_\parallel-\mathbf{q}_\parallel|^2/(2m_0)]-f_0[\varepsilon_m+\hbar^2k_\parallel^2/(2m_0)]\}\\ &\quad+\sum_{\substack{m,n\\ \varepsilon_m>E_F\\ \varepsilon_n>E_F}}\{f_0[\varepsilon_n+\hbar^2|\mathbf{k}_\parallel-\mathbf{q}_\parallel|^2/(2m_0)]-f_0[\varepsilon_m+\hbar^2k_\parallel^2/(2m_0)]\}\Bigg]\overleftrightarrow{\mathbf{D}}_{nm}\frac{d^2k_\parallel}{(2\pi)^2},\end{aligned} \tag{9}$$

where

$$\overleftrightarrow{\mathbf{D}}_{nm}=\frac{e^2\delta(z'-z)\psi_m(z)\psi_n(z)\overleftrightarrow{\mathbf{U}}\mathbf{j}_{nm}(\mathbf{k}_\parallel,\mathbf{k}_\parallel-\mathbf{q}_\parallel,z'')}{2m_0\omega^2[\hbar(\omega+i/\tau)+\varepsilon_n-\varepsilon_m+\hbar^2|\mathbf{k}_\parallel-\mathbf{q}_\parallel|^2/(2m_0)-\hbar^2k_\parallel^2/(2m_0)]}. \tag{10}$$

Approximating the Fermi-Dirac distribution function by its low-temperature form, i.e., $f_0(E)=\vartheta(E_F-E)$, where ϑ is the Heaviside unit step function and E_F is the Fermi energy, one then obtains

$$\begin{aligned}\overleftrightarrow{\mathbf{\Pi}}(z,z',z'')=&\int\Bigg[\sum_{\substack{m,n\\ \varepsilon_m<E_F\\ \varepsilon_n<E_F}}\{f_0[\varepsilon_n+\hbar^2|\mathbf{k}_\parallel-\mathbf{q}_\parallel|^2/(2m_0)]-f_0[\varepsilon_m+\hbar^2k_\parallel^2/(2m_0)]\}+\sum_{\substack{m,n\\ \varepsilon_m>E_F\\ \varepsilon_n<E_F}}\{f_0[\varepsilon_n+\hbar|\mathbf{k}_\parallel-\mathbf{q}_\parallel|^2/(2m_0)]\}\\ &-\sum_{\substack{m,n\\ \varepsilon_m<E_F\\ \varepsilon_n>E_F}}\{f_0[\varepsilon_m+\hbar^2k_\parallel^2/(2m_0)]\}\Bigg]\overleftrightarrow{\mathbf{D}}_{nm}\frac{d^2k_\parallel}{(2\pi)^2}\\ =&\int\Bigg[\sum_{\substack{m,n\\ \varepsilon_m<E_F\\ \varepsilon_n<E_F}}\{f_0[\varepsilon_n+\hbar^2|\mathbf{k}_\parallel-\mathbf{q}_\parallel|^2/(2m_0)]-f_0[\varepsilon_m+\hbar^2k_\parallel^2/(2m_0)]\}\overleftrightarrow{\mathbf{D}}_{nm}\\ &+\sum_{\substack{m,n\\ \varepsilon_m>E_F\\ \varepsilon_n<E_F}}\{f_0[\varepsilon_n+\hbar^2|\mathbf{k}_\parallel-\mathbf{q}_\parallel|^2/(2m_0)]\overleftrightarrow{\mathbf{D}}_{nm}-\{f_0[\varepsilon_n+\hbar^2k_\parallel^2/(2m_0)]\}\overleftrightarrow{\mathbf{D}}_{mn}\Bigg]\frac{d^2k_\parallel}{(2\pi)^2}.\end{aligned} \tag{11}$$

The integrations over the $\mathbf{k}_\parallel$ domain appearing in Eq. (11) can be carried out analytically in the manner described in the Appendix. Choosing $\mathbf{q}_\parallel$ in the x direction, see Fig. 1, the nonzero components of the photon-drag response tensor become

$$\Pi_{xxx}(z,z',z'')=\gamma\delta(z'-z)\Bigg[\sum_{\substack{m,n\\ \varepsilon_m<E_F\\ \varepsilon_n<E_F}}\phi_{nm}(z)\phi_{nm}(z'')(R_-^{(nm)}-R_+^{(nm)})+\sum_{\substack{m,n\\ \varepsilon_m>E_F\\ \varepsilon_n<E_F}}\phi_{nm}(z)\phi_{nm}(z'')(R_-^{(nm)}-R_+^{(mn)})\Bigg], \tag{12}$$

$$\Pi_{xxz}(z,z',z'')=i\gamma\delta(z'-z)\Bigg[\sum_{\substack{m,n\\ \varepsilon_m<E_F\\ \varepsilon_n<E_F}}\phi_{nm}(z)\Phi_{nm}(z'')(H_-^{(nm)}+H_+^{(nm)})+\sum_{\substack{m,n\\ \varepsilon_m>E_F\\ \varepsilon_n<E_F}}\phi_{nm}(z)\Phi_{nm}(z'')(H_-^{(nm)}+H_+^{(mn)})\Bigg] \tag{13}$$

and

$$\Pi_{xxx}(z,z',z'')=\Pi_{yyx}(z,z',z'')=\Pi_{zzx}(z,z',z''), \tag{14}$$

$$\Pi_{xxz}(z,z',z'')=\Pi_{yyz}(z,z',z'')=\Pi_{zzz}(z,z',z''), \tag{15}$$

where

$$\gamma=-\frac{\hbar e^3}{4m_0^2\omega^2}, \tag{16}$$

$$R_\pm^{(nm)}=\frac{1}{2\pi\beta}\Bigg[\frac{1}{\beta}\left(\frac{2\alpha_\pm^{(nm)}}{\beta}\mp q_\parallel\right)\times(\alpha_\pm^{(nm)}-\sqrt{(\alpha_\pm^{(nm)})^2-\beta^2\kappa_{\parallel,\pm}^2})-\kappa_{\parallel,\pm}^2\Bigg], \tag{17}$$

and

$$H_\pm^{(nm)}=\frac{1}{2\pi\beta^2}\,(\alpha_\pm^{(nm)}-\sqrt{(\alpha_\pm^{(nm)})^2-\beta^2\kappa_{\parallel,\pm}^2}) \tag{18}$$

with

$$\alpha_\pm^{(nm)}=\hbar(\omega+i/\tau)+\varepsilon_n-\varepsilon_m\pm\frac{\hbar^2q_\parallel^2}{2m_0}, \tag{19}$$

$$\kappa_{\parallel,+}=\frac{\sqrt{2m_0(E_F-\varepsilon_m)}}{\hbar},\quad \kappa_{\parallel,-}=\frac{\sqrt{2m_0(E_F-\varepsilon_n)}}{\hbar}, \tag{20}$$

and

$$\beta=\frac{\hbar^2}{m_0}\,q_\parallel. \tag{21}$$

In the above equations to obtain the two quantities $R_+^{(mn)}$ and $H_+^{(mn)}$, one has to interchange the supscript $n\leftrightarrow m$ and thus $\kappa_{\parallel,+}$ with $\kappa_{\parallel,-}$ in Eqs. (17)–(20).

Among the twenty-seven elements of the second order photon-drag response tensor only six are nonvanishing. The six elements fall in two groups, each containing three identical elements. The symmetry scheme of the response tensor is shown in Fig. 2. Due to the presence of the Dirac δ function in Eqs. (12) and (13), the photon-drag response tensor is a so-called semilocal tensor. The contribution to $\overleftrightarrow{\Pi}(z,z',z'')$ from the intrasubband transitions are given by the terms in Eqs. (12) and (13) for which $m=n$. Since

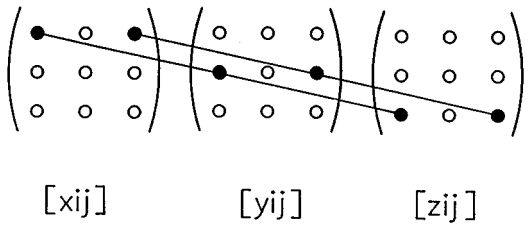

FIG. 2. Symmetry scheme of the semilocal photon-drag response tensor.

$\Phi_{nn}(z)=0$, it appears that only the elements in Eq. (14) contribute to the intrasubband photon drag. This is in agreement with the results obtained for a one-level quantum well in Ref. 4, and the result is obvious since intrasubband transitions can only give rise to a transition current density in the plane of the well. The presence of intersubband transitions means that the transition current density attains a component perpendicular to the well plane, and therefore the three elements in Eq. (15) show up only in the context of intersubband dynamics. The intersubband transitions of course contribute to the elements in Eq. (14) also. It is easy to demonstrate that $R_{\pm}^{(nm)}\rightarrow 0$ for $\mathbf{q}_{\parallel}\rightarrow 0$. This means that $\Pi_{xxx}(z,z',z'')$ [and also $\Pi_{yyx}(z,z',z'')$ and $\Pi_{zzx}(z,z',z'')$] vanishes in the local (loc), i.e., $\mathbf{q}_{\parallel}\rightarrow 0$, limit. The physical reason for this originates in the fact that excitations along the well require a net momentum exchange between the field and particle system, as mentioned also in Ref. 4. A net momentum transfer is not required for excitations perpendicular to the plane of the well, and therefore $\Pi_{xxz}(z,z',z'')$ [and also $\Pi_{yyz}(z,z',z'')$ and $\Pi_{zzz}(z,z',z'')$] is different from zero

$$\{(H_{\pm}^{(nm)})_{\mathrm{loc}}=m_0(E_F-\varepsilon_n)/\{2\pi\hbar^2[\hbar(\omega+i/\tau)+\varepsilon_n-\varepsilon_m]\}\}.$$

For p-polarized light, the two elements containing the index y, namely, $\Pi_{yyx}(z,z',z'')$ and $\Pi_{yyz}(z,z',z'')$, do not contribute to the drag phenomenon, and if the incident field is s polarized the photon-drag effect is absent.

Finally, by substituting Eqs. (12)–(15) into Eq. (6), one finds that the photon-drag current density along the quantum well is given by

$$\begin{aligned}J_{0,x}(z)\mathbf{e}_x&=(\overleftrightarrow{\mathbf{U}}-\mathbf{e}_z\mathbf{e}_z)\cdot\mathbf{J}_0(z)\\&=\Bigg(\sum_{m,n}^{\substack{\varepsilon_n<E_F\\ \varepsilon_m<E_F}}\left\{\frac{\gamma}{2}E_x^*(z)\phi_{nm}(z)\left[(R_-^{(nm)}-R_+^{(nm)})\int E_x(z')\phi_{nm}(z')dz'+i(H_-^{(nm)}+H_+^{(nm)})\int E_z(z')\Phi_{nm}(z')dz'\right]+\mathrm{c.c.}\right\}\\&\quad+\sum_{m,n}^{\substack{\varepsilon_n<E_F\\ \varepsilon_m>E_F}}\left\{\frac{\gamma}{2}E_x^*(z)\phi_{nm}(z)\left[(R_-^{(nm)}-R_+^{(mn)})\int E_x(z')\phi_{nm}(z')dz'+i(H_-^{(nm)}+H_+^{(mn)})\right.\right.\\&\quad\left.\left.\times\int E_z(z')\Phi_{nm}(z')dz'\right]+\mathrm{c.c.}\right\}\Bigg)\mathbf{e}_x+(\overleftrightarrow{\mathbf{U}}-\mathbf{e}_z\mathbf{e}_z)\cdot\mathrm{Tr}\{\rho_{\mathrm{NL}}^{(0)}\mathbf{j}_0\}.\end{aligned}\tag{22}$$

By integrating Eq. (22) across the quantum well and by using Eq. (5), the photon-drag current along the quantum well, i.e., $I_0=\int_{-d}^{0}J_{0,x}(z)dz$, becomes

$$\begin{aligned}I_0=\gamma\,\mathrm{Re}\Bigg\{&\sum_{m,n}^{\substack{\varepsilon_n<E_F\\ \varepsilon_m<E_F}}\left[(R_-^{(nm)}-R_+^{(nm)})\left|\int E_x(z)\phi_{nm}(z)dz\right|^2+i(H_-^{(nm)}+H_+^{(nm)})\int E_x^*(z)\phi_{nm}(z)dz\int E_z(z)\Phi_{nm}(z)dz\right]\\&+\sum_{m,n}^{\substack{\varepsilon_n<E_F\\ \varepsilon_m>E_F}}\left[(R_-^{(nm)}-R_+^{(mn)})\left|\int E_x(z)\phi_{nm}(z)dz\right|^2+i(H_-^{(nm)}+H_+^{(mn)})\int E_x^*(z)\phi_{nm}(z)dz\int E_z(z)\Phi_{nm}(z)dz\right]\Bigg\}.\end{aligned}\tag{23}$$

B. Photon-drag response in a two-level model

In Sec. II A we have derived the general expression for the photon-drag response function and the explicit expression for the photon-drag current. In this subsection we shall restrict ourselves to the situation in which there are only two bound states in the quantum well, and assume that only the ground state is populated. It is known that there exist three kinds of possible transitions in the quantum well, namely, (i) transitions in the same band, say n, and $\varepsilon_n<E_F$, (ii) transitions between different bands, say n and m, with $\varepsilon_n<E_F$ and $\varepsilon_m<E_F$, (iii) transitions between different bands, n and m, with $\varepsilon_n<E_F$ and $\varepsilon_m>E_F$. In case (i) only the first sum in Eq. (12) contributes and there are hence only three nonzero elements in the response tensor. For case (ii), since the transitions involve different levels, the first sum on the right-hand side of both Eqs. (12) and (13) is different from zero, and there thus are six nonzero elements in the response tensor. In case (iii) only the second sums on the right-hand sides of Eqs. (12) and (13) are present.

In the remaining part of the paper we consider only case (iii). The level being below the Fermi energy is denoted by

subscript a, and the other (above the Fermi level) is denoted by b. From the general expression [Eq. (23)] for the photon-drag current one then obtains

$$I_0=\gamma\ \mathrm{Re}\Big[(R_-^{(ab)}-R_+^{(ba)})\Big|\int E_x(z)\phi_{ab}(z)dz\Big|^2 + i(H_-^{(ab)}+H_+^{(ba)})\int E_x^*(z)\phi_{ab}(z)dz \times\int E_z(z)\Phi_{ab}(z)dz\Big]. \tag{24}$$

In order to complete the calculation of the photon-drag effect in the quantum well, we still need to determine the local electric field inside the well.

III. LOCAL FIELD IN A TWO-LEVEL QUANTUM WELL

Since only the p-polarized electric field is involved in the intersubband transition process, for simplicity in the following we omit the y component of the electric field in our analysis. This means that vectors are two-component quantities and tensors 2×2 matrices. By taking as a starting point a Green's function description, the local field in the well satisfies the following vectorial integral equation:[10,12]

$$\mathbf{E}(z)=\mathbf{E}^B(z)-i\mu_0\omega\int\int\overleftrightarrow{\mathbf{G}}(z,z')\cdot\overleftrightarrow{\boldsymbol{\sigma}}(z',z'')\cdot\mathbf{E}(z'')dz''dz', \tag{25}$$

where $\mathbf{E}^B(z)$ denotes the so-called background field consisting of the sum of the incident field and the field reflected from the substrate in the absence of the quantum well. The appropriate electromagnetic propagator $\overleftrightarrow{\mathbf{G}}(z,z')$ is given by

$$\overleftrightarrow{\mathbf{G}}(z,z')=\frac{1}{2iq_\perp}\{\exp(iq_\perp|z-z'|)[\vartheta(z-z')\mathbf{e}_i\mathbf{e}_i+\vartheta(z'-z)\mathbf{e}_r\mathbf{e}_r]+r^p\exp[-iq_\perp(z+z')]\mathbf{e}_r\mathbf{e}_i\}+\left(\frac{c_0}{\omega}\right)^2\delta(z'-z)\mathbf{e}_z\mathbf{e}_z, \tag{26}$$

where $\mathbf{e}_i=(c_0/\omega)(q_\perp,-q_\parallel)$, $\mathbf{e}_r=(c_0/\omega)(-q_\perp,-q_\parallel)$, c_0 is the light speed in vacuum, and r^p is the p-polarized amplitude reflection coefficient, which is given by $r^p=(q_\perp\varepsilon_Q-k_\perp)/(q_\perp\varepsilon_Q+k_\perp)$ with $k_\perp=\sqrt{(\omega/c_0)^2\varepsilon_Q-q_\parallel^2}$ being the z component of the wave vector in the substrate, and ε_Q the dielectric constant of the substrate. In the long wavelength limit the conductivity tensor entering Eq. (25) is given by

$$\overleftrightarrow{\boldsymbol{\sigma}}(z',z'')=\frac{2i}{\omega}\int\sum_{m,n}\left(\frac{\hbar\omega}{\varepsilon_m-\varepsilon_n}\right)\frac{f_0[\varepsilon_n+\hbar^2k_\parallel^2/(2m_0)]-f_0[\varepsilon_m+\hbar^2k_\parallel^2/(2m_0)]}{\hbar(\omega+i/\tau)+\varepsilon_n-\varepsilon_m}\mathbf{j}_{mn}(\mathbf{k}_\parallel,\mathbf{k}_\parallel,z')\mathbf{j}_{nm}(\mathbf{k}_\parallel,\mathbf{k}_\parallel,z'')\frac{d^2k_\parallel}{(2\pi)^2}, \tag{27}$$

in dyadic notation. The presence of the factor $\hbar\omega/(\varepsilon_m-\varepsilon_n)$ indicates that both the diamagnetic and paramagnetic parts are incorporated in $\overleftrightarrow{\boldsymbol{\sigma}}(z',z'')$.

In the present context it is sufficient to approximate $\overleftrightarrow{\boldsymbol{\sigma}}(z',z'')$ by its low-temperature form. By carrying out next the integration in Eq. (27), one finds that the conductivity tensor of our two-band model is diagonal, with the nonzero elements given by

$$\sigma_{xx}(z',z'')=\frac{ie^2}{\pi\hbar}\frac{(E_F-\varepsilon_a)^2}{[\hbar(\omega+i/\tau)]^2-(\varepsilon_b-\varepsilon_a)^2}\phi(z')\phi(z''), \tag{28}$$

$$\sigma_{zz}(z',z'')=\frac{i\hbar e^2}{2\pi m_0}\frac{(E_F-\varepsilon_a)}{[\hbar(\omega+i/\tau)]^2-(\varepsilon_b-\varepsilon_a)^2}\Phi(z')\Phi(z''). \tag{29}$$

For simplicity, here and below, we omit writing the subscripts on the wave function combinations, i.e., $\phi(z)\equiv\phi_{ab}(z)$ and $\Phi(z)\equiv\Phi_{ab}(z)$.

The diagonal form of $\overleftrightarrow{\boldsymbol{\sigma}}(z',z'')$, plus the fact that both $\sigma_{xx}(z',z'')$ and $\sigma_{zz}(z',z'')$ consist of products of functions of z' and z'', respectively, allows one to rewrite Eq. (25) in the form

$$\mathbf{E}(z)=\mathbf{E}^B(z)+\overleftrightarrow{\boldsymbol{\Xi}}(z)\cdot\boldsymbol{\eta}, \tag{30}$$

where

$$\overleftrightarrow{\boldsymbol{\Xi}}(z)=\left[\int\overleftrightarrow{\mathbf{G}}(z,z')\cdot\overleftrightarrow{\mathbf{T}}(z')dz'\right]\cdot\overleftrightarrow{\boldsymbol{\Theta}}, \tag{31}$$

$$\boldsymbol{\eta}=\int\overleftrightarrow{\mathbf{T}}(z)\cdot\mathbf{E}(z)dz, \tag{32}$$

with

$$\overleftrightarrow{\mathbf{T}}(z)=\begin{pmatrix}\phi(z)&0\\0&\Phi(z)\end{pmatrix}, \tag{33}$$

and

$$\overleftrightarrow{\boldsymbol{\Theta}}=\begin{pmatrix}\Theta_{xx}&0\\0&\Theta_{zz}\end{pmatrix}, \tag{34}$$

the elements of $\overleftrightarrow{\boldsymbol{\Theta}}$ being given by

$$\Theta_{xx}=\frac{\mu_0e^2\omega}{\pi\hbar}\frac{(E_F-\varepsilon_a)^2}{[\hbar(\omega+i/\tau)]^2-(\varepsilon_b-\varepsilon_a)^2}, \tag{35}$$

$$\Theta_{zz}=\frac{\mu_0 e^2\hbar\omega}{2\pi m_0}\frac{(E_F-\varepsilon_a)}{[\hbar(\omega+i/\tau)]^2-(\varepsilon_b-\varepsilon_a)^2}. \tag{36}$$

Written in the form given in Eq. (30), the integral equation for the local field is easily solved by standard techniques. Then, by multiplying Eq. (30) with $\overleftrightarrow{\mathbf{T}}(z)$ from the left, and thereafter performing a z integration of the resulting equation, one finds that the unknown vector $\boldsymbol{\eta}=(\eta_x,\eta_z)$ can be obtained from the matrix equation

$$(\overleftrightarrow{\mathbf{U}}-\overleftrightarrow{\mathbf{P}})\cdot\boldsymbol{\eta}=\mathbf{N}, \tag{37}$$

where

$$\mathbf{N}=\begin{pmatrix}N_x\\N_z\end{pmatrix}=\int\overleftrightarrow{\mathbf{T}}(z)\cdot\mathbf{E}^B(z)dz \tag{38}$$

and

$$\overleftrightarrow{\mathbf{P}}=\begin{pmatrix}P_{xx}&P_{xz}\\P_{zx}&P_{zz}\end{pmatrix}=\int\overleftrightarrow{\mathbf{T}}(z)\cdot\overleftrightarrow{\boldsymbol{\Xi}}(z)dz. \tag{39}$$

At this point we need to specify the wave functions and energies of the two bands. Hence, by using the wave functions of the simple infinite-barrier model, one finds that the parameters appearing in Eq. (37) are given by

$$P_{xx}=-\frac{\Theta_{xx}c_0^2q_\perp^2d}{2\omega^2}\left\{\left[\frac{1}{(\kappa_+\pi)^2-(q_\perp d)^2}+\frac{1}{(\kappa_-\pi)^2-(q_\perp d)^2}\right]+iq_\perp d[1+\exp(iq_\perp d)]\{2+r^p[1+\exp(iq_\perp d)]\}\right.$$
$$\left.\times\left[\frac{1}{(\kappa_+\pi)^2-(q_\perp d)^2}-\frac{1}{(\kappa_-\pi)^2-(q_\perp d)^2}\right]^2\right\}, \tag{40}$$

$$P_{zx}=-\frac{\Theta_{xx}}{\Theta_{zz}}P_{xz}$$
$$=-\frac{\Theta_{xx}\kappa_-\kappa_+\pi^2c_0^2q_\parallel}{2id\omega^2}\left\{\left[\frac{1}{(\kappa_+\pi)^2-(q_\perp d)^2}+\frac{1}{(\kappa_-\pi)^2-(q_\perp d)^2}\right]+iq_\perp d[1+\exp(iq_\perp d)]\{2-r^p[1+\exp(iq_\perp d)]\}\right.$$
$$\left.\times\left[\frac{1}{(\kappa_+\pi)^2-(q_\perp d)^2}-\frac{1}{(\kappa_-\pi)^2-(q_\perp d)^2}\right]^2\right\}, \tag{41}$$

$$P_{zz}=\frac{\Theta_{zz}\pi^2c_0^2}{\omega^2d^3}\left(\frac{\kappa_-^2+\kappa_+^2}{2}\right)+\frac{\Theta_{zz}\kappa_-^2\kappa_+^2\pi^4c_0^2q_\parallel^2}{2iq_\perp d^2\omega^2}\left\{\frac{q_\perp d}{i\pi^2\kappa_-^2\kappa_+^2}\left[\frac{\kappa_+^2}{(\kappa_-\pi)^2-(q_\perp d)^2}+\frac{\kappa_-^2}{(\kappa_+\pi)^2-(q_\perp d)^2}\right]\right.$$
$$\left.+[1+\exp(iq_\perp d)]\{2+r^p[1+\exp(iq_\perp d)]\}\left[\frac{1}{(\kappa_-\pi)^2-(q_\perp d)^2}-\frac{1}{(\kappa_+\pi)^2-(q_\perp d)^2}\right]^2\right\}, \tag{42}$$

and

$$N_x=-iq_\perp d\cos\theta\{1+\exp(iq_\perp d)+r^p[1+\exp(iq_\perp d)]\}$$
$$\times\left[\frac{1}{(\kappa_+\pi)^2-(q_\perp d)^2}-\frac{1}{(\kappa_-\pi)^2-(q_\perp d)^2}\right], \tag{43}$$

$$N_z=\frac{\kappa_+\kappa_-\pi^2}{d^2}\sin\theta\{1+\exp(iq_\perp d)+r^p[1+\exp(iq_\perp d)]\}$$
$$\times\left[\frac{1}{(\kappa_+\pi)^2-(q_\perp d)^2}-\frac{1}{(\kappa_-\pi)^2-(q_\perp d)^2}\right], \tag{44}$$

where $\kappa_-=b-a$ and $\kappa_+=a+b$, a and b being the quantum numbers of the two states in consideration. The quantum numbers enter in the wave functions as follows: $\psi_m(z)=-(2/d)^{1/2}\sin(m\pi z/d)$, $m=a,b$.

IV. PHOTON DRAG IN MULTIPLE QUANTUM-WELL SYSTEMS

In this section we consider the photon drag in a multiple quantum-well structure which consists of M wells embedded in an infinitely extended homogeneous and isotropic medium. For a multiple well system Eq. (25) must thus be replaced by the integral equation

$$\mathbf{E}(z)=\mathbf{E}^B(z)-i\mu_0\omega\times\sum_{j=1}^{M}\int\int\overleftrightarrow{\mathbf{G}}(z-z')\cdot\boldsymbol{\sigma}^{(j)}(z',z'')\cdot\mathbf{E}(z'')dz''dz', \tag{45}$$

where $\overleftrightarrow{\mathbf{G}}(z-z')$ is the direct part of the electromagnetic propagator in Eq. (26), and $\overleftrightarrow{\boldsymbol{\sigma}}^{(j)}(z',z'')$ is the conductivity tensor of the jth well.

Following the same procedure as discussed in the previous section and assuming that in each well there are two bound states, of which only the lower one is populated, we can rewrite Eq. (45) as

$$\mathbf{E}(z)=\mathbf{E}^{B}(z)+\sum_{j=1}^{M}\overleftrightarrow{\Xi}^{(j)}(z)\cdot\boldsymbol{\eta}^{(j)}, \tag{46}$$

where $\overleftrightarrow{\Xi}^{(j)}(z)=[\int\overleftrightarrow{\mathbf{G}}(z-z')\cdot\overleftrightarrow{\mathbf{T}}^{(j)}(z')dz']\cdot\overleftrightarrow{\Theta}$. The yet unknown vectors $\boldsymbol{\eta}^{(i)}$ satisfy the algebraic relation

$$\overleftrightarrow{\mathbf{U}}\cdot\boldsymbol{\eta}^{(i)}-\sum_{j=1}^{M}\overleftrightarrow{\mathbf{P}}^{(i,j)}\cdot\boldsymbol{\eta}^{(j)}=\mathbf{N}^{(i)},\quad i=1,2,\ldots,M, \tag{47}$$

where $\overleftrightarrow{\mathbf{P}}^{(i,j)}=\int\overleftrightarrow{\mathbf{T}}^{(i)}(z)\cdot\overleftrightarrow{\Xi}^{(j)}(z)dz=[\int\overleftrightarrow{\mathbf{T}}^{(i)}(z)\cdot\int\overleftrightarrow{\mathbf{G}}(z-z')\cdot\overleftrightarrow{\mathbf{T}}^{(j)}(z')dz'dz]\cdot\overleftrightarrow{\Theta}$ and $\mathbf{N}^{(i)}=\int\overleftrightarrow{\mathbf{T}}^{(i)}(z)\cdot\mathbf{E}^{B}(z)dz$. For each of the indices $i=1,2,\ldots,M$ a new relation is obtained, and together these relations constitute sufficient equations to determine the various $\boldsymbol{\eta}^{(i)}$'s. The induced radiative coupling between the wells appear via the $\overleftrightarrow{\mathbf{P}}^{(i,j)}$'s for which $i\neq j$. If we neglect the radiative coupling among the wells, the $\boldsymbol{\eta}^{(i)}$'s are determined via

$$\overleftrightarrow{\mathbf{U}}\cdot\boldsymbol{\eta}^{(i)}-\overleftrightarrow{\mathbf{P}}^{(i,i)}\cdot\boldsymbol{\eta}^{(i)}=\mathbf{N}^{(i)},\quad i=1,2,\ldots,M. \tag{48}$$

Since the quantum wells are assumed to be electronically isolated, the induced photon-drag current in the system is just the sum of the currents of the individual wells, i.e.,

$$I_0=\gamma\,\mathrm{Re}\left\{\sum_{j=1}^{M}\left[(R_{-,j}^{(ab)}-R_{+,j}^{(ba)})\left|\int E_x(z)\phi_{ab}^{(j)}(z)dz\right|^2\right.\right.$$
$$+i(H_{-,j}^{(ab)}+H_{+,j}^{(ba)})\int E_x^{*}(z)\phi_{ab}^{(j)}(z)dz$$
$$\left.\left.\times\int E_z(z)\Phi_{ab}^{(j)}(z)dz\right]\right\}, \tag{49}$$

in an obvious notation.

V. NUMERICAL CALCULATION AND DISCUSSION

A. Photon drag in a single quantum well

In this subsection numerical calculations of the photon-drag current in a vacuum/niobium/quartz quantum-well system are presented. For this system local-field calculations of (i) the s- and p-polarized linear reflection coefficients, (ii) the electromagnetic surface wave dispersion relations, (iii) the optical second-harmonic generation, and (iv) intrasubband (one-level) photon drag have already been carried out, and the experimental studies of the s-polarized reflection coefficient, the surface wave dispersion relations, and the second-harmonic generation show qualitative agreement with the theory. For a general review of these effects the reader is referred to Ref. 12.

We choose the two levels in such a manner that the Fermi energy is located in between them, and the range of the light frequencies used are so close to the interlevel transition frequency that the two-level model is a good approximation. The thickness of the niobium well is in all cases $d=15$ Å. The quantum numbers of the chosen states are $a=5$ and $b=6$, and the corresponding energy separation is $\varepsilon_{ba}=1.8380$ eV. The Fermi energy is 5.32 eV. The frequency dependence of the dielectric constant of the quartz substrate (ε_Q) are as in Ref. 13, and the relaxation energy used in Figs. 3–9 is $\hbar/\tau=0.6$ meV. Since the photon-drag current is proportional to the square of the amplitude of the incident (inc) field E_{inc}, it is adequate to normalize the photon drag data with the magnitude of the time-averaged Poynting vector of the incident field $S_{\mathrm{inc}}=\varepsilon_0 c_0|E_{\mathrm{inc}}|^2/2$. The normalized photon-drag current hence is given by

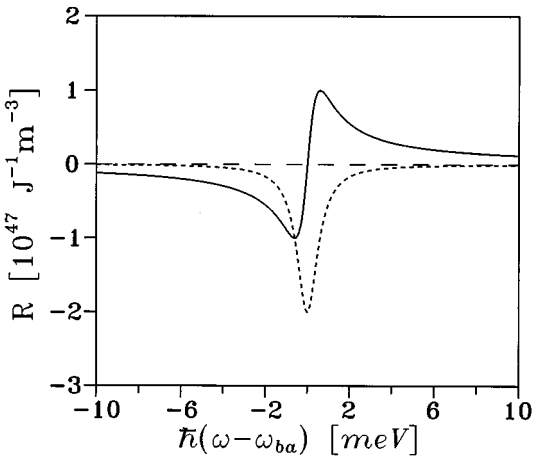

FIG. 3. Photon-drag response function $R=R_{-}^{(ab)}-R_{+}^{(ba)}$ as a function of the incident photon energy measured from the electronic transition energy $\hbar\omega_{ba}$. The solid and dashed lines represent the real and imaginary parts of R, respectively. The angle of incidence is 60°.

$$\frac{I_0}{S_{\mathrm{inc}}}=\frac{2\gamma}{\varepsilon_0 c_0|E_{\mathrm{inc}}|^2}\,\mathrm{Re}[R|\eta_x|^2+iH\eta_x^{*}\eta_z], \tag{50}$$

with the abbreviations $R=R_{-}^{(ab)}-R_{+}^{(ba)}$ and $H=H_{+}^{(ba)}+H_{-}^{(ab)}$.

It is instructive first to study the behavior of R and H of Eq. (50). In Figs. 3 and 4 we thus plot R and H as functions of the incident photon energy, using an angle of incidence of 60°. It appears that both R and H exhibit a resonance behavior around ε_{ba}. To compare the contribution from the first and second terms on the right-hand side of Eq. (50), we notice that $|\eta_x|\approx|\eta_z|d$. This implies that we have to compare the two quantities $|R|$ and $|H|/d$. Since $d\approx10^{-9}$ m, it appears from Figs. 3 and 4 that $|H|/d$ is two orders of magnitude larger than $|R|$. Therefore, the second term in Eq. (50) gives the dominating contribution to the photon-drag current.

We know from our previous discussion that $|R|=0$ in the local limit. Here we shall investigate H in the local (loc) limit. Thus, in Fig. 5 we show the difference between H and H_{loc} as a function of the photon energy for two different angles of incidence, namely, $\theta=60°$ (curves 1) and $\theta=30°$ (curves 2). The solid and dashed lines represent the real and imaginary parts of $H-H_{\mathrm{loc}}$, respectively. It is clear from Fig. 5 that the local approximation for H is extremely good [the relative difference $(H-H_{\mathrm{loc}})/H$ being less than 0.01]. When the angle of incidence decreases, the difference H

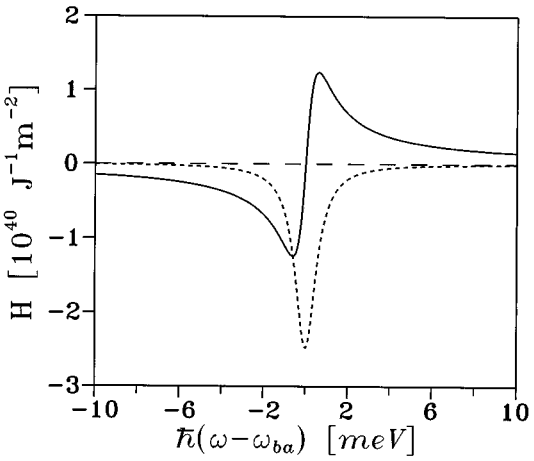

FIG. 4. Photon-drag response function $H=H_{-}^{(ab)}+H_{+}^{(ba)}$ as a function of the incident photon energy measured from the electronic transition energy $\hbar\omega_{ba}$. The solid and dashed lines represent the real and imaginary parts of H, respectively. The angle of incidence is 60°.

$-H_{\rm loc}$ becomes smaller. This is so because $q_{\|}$ also gets smaller. In the limit $\theta\rightarrow 0$, $H\rightarrow H_{\rm loc}$.

In Fig. 6(a) the normalized photon-drag current is plotted as a function of the incident photon energy for different angles of incidence. The solid lines show the results (I_0) obtained when local-field corrections are included, and the dashed lines represent the results (I_B) without the local-field corrections. The angles of incidence are 50°(curves 1), 60°(curves 2), and 70°(curves 3). It appears from Fig. 6(a) that the photon-drag current shows two distinct resonance peaks in which the currents flow in opposite directions. Without the local-field corrections, the current is antisymmetric with respect to ε_{ba}, and when the incident photon energy is less than the energy separation ε_{ba}, the current flows in the negative x direction, and for $\hbar\omega>\varepsilon_{ba}$ the flow

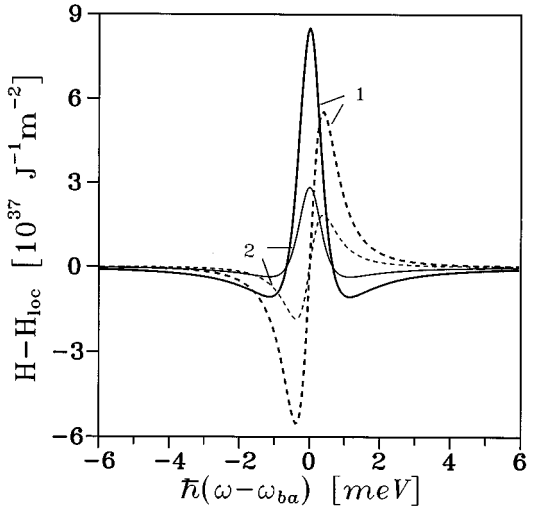

FIG. 5. Difference between H and $H_{\rm loc}$ as a function of the photon energy measured from the transition energy $\hbar\omega_{ba}$ for two different angles of incidence $\theta=60°$ (curves 1), $\theta=30°$ (curves 2). The real and imaginary parts of $H-H_{\rm loc}$ are plotted in the solid and dashed lines, respectively.

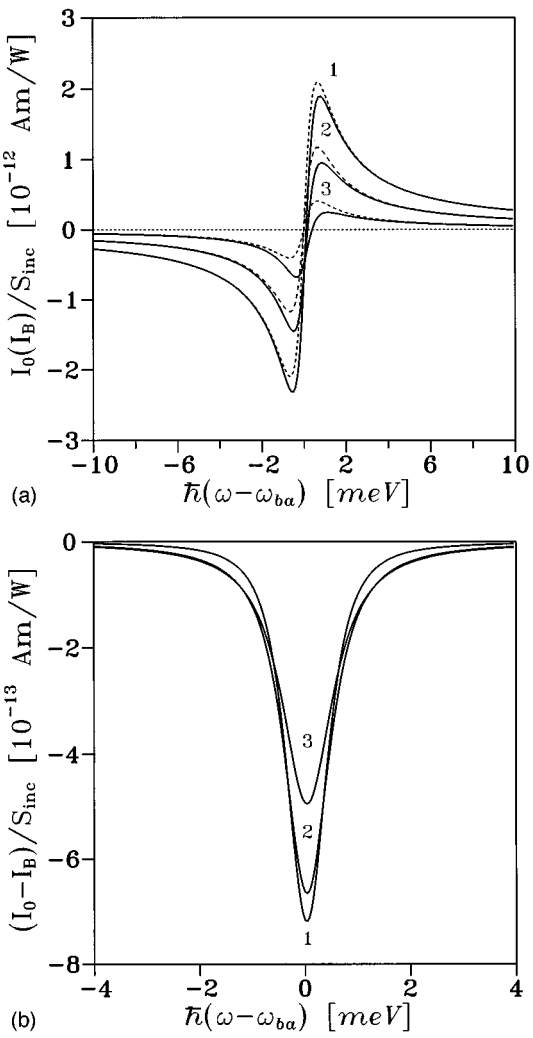

FIG. 6. (a). Photon-drag current normalized with the magnitude of the incident Poynting vector as a function of the incident photon energy measured from $\hbar\omega_{ba}$ for different angles of incidence. The results with and without the local-field corrections are plotted in solid and dashed lines, respectively. The angles of incidence are 50° (curves 1), 60° (curves 2), and 70° (curves 3). (b) Difference between the drag currents (normalized with the magnitude of the incident Poynting vector) with (I_0) and without (I_B) local-field effects incorporated as a function of the photon energy (measured from $\hbar\omega_{ba}$) for three different angles of incidence, viz., 50° (curves 1), 60° (curves 2), and 70° (curves 3).

is in the positive x direction. Neglect of local-field effects means that the field is equal to the background field so that $\boldsymbol{\eta}=\mathbf{N}$. In the frequency range around $\hbar\omega_{ba}\approx 1.8380$ eV, the reflection coefficient r^p is almost real, and this implies that the product $(N_x^* N_z)$ is almost a purely imaginary number [see Eqs. (43) and (44)]. The form of the photon-drag current hence reflects the frequency behavior of the real part of H (compare Figs. 4 and 6). From our numerical calculation it turns out that the local field inside the quantum well can be highly nonuniform, and thus the local-field corrections which appears in the $\boldsymbol{\eta}$ parameters can produce major changes in the calculated photon-drag current in the quantum-well system. A quantitative comparison of the frequency dependence of the photon-drag current with and without (i.e., with $\boldsymbol{\eta}$

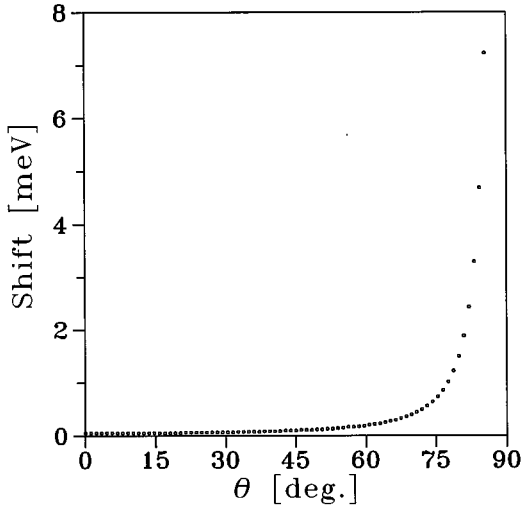

FIG. 7. Blueshift of the zero point of the photon-drag current as a function of the angle of incidence.

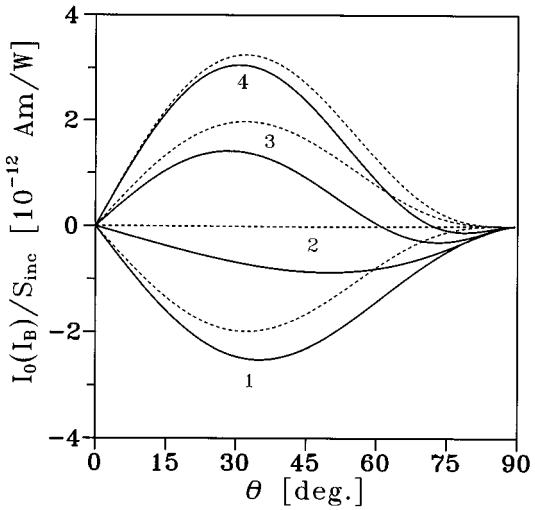

FIG. 8. Photon-drag current normalized to the magnitude of the incident Poynting vector plotted as a function of the angle of incidence for different incident photon energies, viz., 1.8378 eV (curves 1), 1.8380 eV (curves 2), 1.8382 eV (curves 3), and 1.8385 eV (curves 4). Results with and without the local-field corrections are plotted in solid and dashed lines, respectively.

$=\mathbf{N}$) local-field corrections is shown in Fig. 6(b), where the difference between the drag currents with (I_0) and without (I_B) local-field effects incorporated is plotted in normalized form for the same angles of incidence as in Fig. 6(a). Also the remaining input data are as in the previous figure. It appears from this figure that the local-field corrections are particularly important around the electronic resonance. Local-field effects also give rise to a blueshift of the drag current spectra.

In Fig. 7 we plot the blueshift of the zero point of the photon-drag current as a function of the angle of incidence. It appears from this figure that the shift increases monotonically with θ. When the angle of incidence is larger than, say, 75°, the shift is significant, and increases rapidly as a function of the angle of incidence. We know that with the increase of the incident angle, the z component of the local field, which is mainly responsible for the intersubband transitions, increases and this makes the intersubband transition process more probable. As a result the need for taking local-field corrections into account becomes more important with increasing θ.

In Fig. 8 the normalized photon-drag current is plotted as a function of the angle of incidence for various incident photon energies, viz., 1.8378 eV (curves 1), 1.8380 eV (curves 2), 1.8382 eV (curves 3), and 1.8385 eV (curves 4). Results with and without the inclusion of local-field corrections are plotted in solid and dashed lines, respectively. In the limit $\theta\rightarrow 0$, the z component of the local field must vanish so that $|\eta_z|\rightarrow 0$ and since also $|R|\rightarrow 0$ for $q_{\|}\rightarrow 0$, the photon-drag current must be zero for $\theta=0$. This is also obvious for symmetry reasons. For $\theta\rightarrow\pi/2$, the x component of the local field approaches zero, and in turn this implies that $|\eta_x|\rightarrow 0$. The photon-drag current therefore goes to zero for $\theta=\pi/2$. It also appears from Fig. 8 that the location of the normalized maximum of the drag current depends on the photon energy. Since the photon-drag response function H does not change very much with the angle of incidence, the maximum in the drag current is mainly determined by the quantity $\eta_x^*\eta_z$. At $\hbar\omega=\varepsilon_{ba}$ (curves 2) the current is zero, unless local-field effects are included. These effects give rise to a current flow in the negative x direction for all angles of incidence. It is worthwhile to note that for curves 3 and 4 the drag current changes sign at a certain (large) angle of incidence. This is so because the local-field corrections shift the photon-drag current spectrum upwards in energy.

In Fig. 9 the normalized current difference $(I_0-I_B)/S_{\mathrm{inc}}$ is plotted as a function of the angle of incidence. The photon energies are 1.8375 eV (curve 1), 1.8378 eV (curve 2), 1.8382 eV (curve 3), 1.8385 eV (curve 4), and 1.8390 eV (curve 5). It appears from Fig. 9 that when the incoming photon energy is close to the electronic energy separation

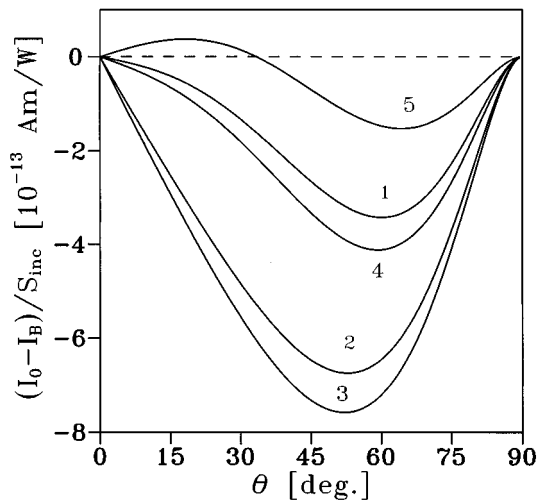

FIG. 9. Difference between the drag currents (normalized with the magnitude of the incident Poynting vector) with (I_0) and without (I_B) local-field effects incorporated as a function of the angle of incidence for different photon energies, viz., 1.8375 eV (curve 1), 1.8378 eV (curve 2), 1.8382 eV (curve 3), 1.8385 eV (curve 4), and 1.8390 eV (curve 5).

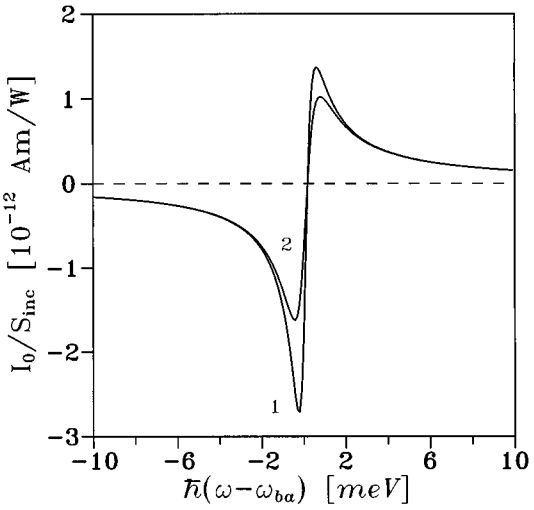

FIG. 10. Photon-drag current normalized by the magnitude of the incident Poynting vector as a function of the photon energy (measured from $\hbar\omega_{ba}$) for two different relaxation energies, viz., $\hbar/\tau=0.4$ meV (curve 1) and 0.6 meV (curve 2). The angle of incidence is $\theta=60°$.

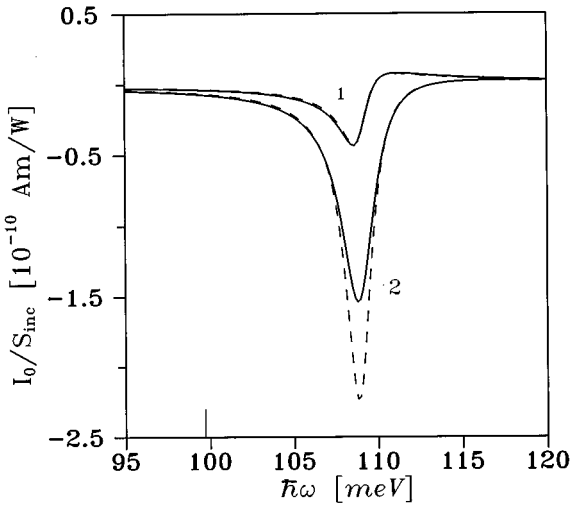

FIG. 11. Photon-drag current normalized by the magnitude of the incident Poynting vector as a function of the photon energy. The solid and dashed lines are the results with and without inclusion of radiative coupling among the wells, respectively. The angles of incidence are 20° (curve 1) and 60° (curve 2), the number of wells is 10, $\Delta=400$ Å, and the tick bar denotes the electronic resonance energy.

ε_{ba} (curves 2 and 3) one can expect a particularly pronounced difference in the predicted (I_0, I_B) currents. This fact is in agreement with the remarks accompanying Fig. 6(b).

In Fig. 10 we show the normalized photon-drag current as a function of the incident photon energy for two different relaxation energies, namely, $\hbar/\tau=0.4$ meV (curve 1) and 0.6 meV (curve 2). The angle of incidence is $\theta=60°$. The numerical results demonstrate that the heights of the resonance peaks in the photon-drag current are very sensitive to the (chosen) value of the relaxation energy. A change in the relaxation energy does not shift the spectrum, however. By varying the relaxation energy, the magnitudes of both the photon-drag response function and the two quantities η_x and η_z are changed.

B. Photon drag in multiple quantum wells

To illustrate the importance of the radiative coupling among quantum wells we have carried out numerical studies of the drag current in a GaAs/Al_xGa_{1-x}As multiple quantum well structure consisting of identical wells. The used input data for the system are as follows. Effective electron mass: $m_0=0.067m_e$ (m_e being the free electron mass), quantum-well width: $d=130$ Å, quantum numbers of the two bound states: $a=1$ and $b=2$, relaxation energy: $\hbar/\tau=1.0$ meV, conduction electron number per unit area: $N_s=1.0\times10^{12}$ cm^{-2} (from this number the distance of the Fermi level from the lower lying level is calculated using the formula $E_F-\varepsilon_1=\pi\hbar^2N_s/m_0$), energy separation between the two bound states: $\varepsilon_{21}=99.7$ meV (using the infinite barrier model), relative dielectric constant of the Al_xGa_{1-x}As medium in the vicinity of the transition frequency: $\varepsilon_Q=13.1$. For convenience we have also for the multiple-well case normalized the drag current data with the magnitude of the time-averaged Poynting vector of the incident field here, $S_{inc}=\varepsilon_0c_0\sqrt{\varepsilon_Q}|E_{inc}|^2/2$.

In Fig. 11 we show the normalized photon-drag current as a function of the incident photon energy with (solid lines) and without (dashed lines) inclusion of the radiative coupling among the wells. The angles of incidence are 20° (curve 1) and 60° (curve 2), the spatial period of the multiple quantum-well system is $\Delta=400$ Å, and the number of wells is 10. The tick bar denotes the electronic resonance energy. It appears from Fig. 11 that when the angle of incidence is small (curve 1), the radiative coupling is not important. However, when the angle of incidence is large (curve 2), a neglect of the radiative coupling may lead to a significant overestimation of the magnitude of the drag current near resonance. It was apparent from the results presented in Fig. 6(a) that the local-field corrections destroy the antisymmetric form of the frequency dependence of the drag current near resonance, the general tendency being that the magnitude of the peak lying on the high-frequency side of the resonance is reduced, while the magnitude of the other peak becomes larger. In the multiple quantum-well case this asymmetry becomes more pronounced particularly for large angles of incidence, and the high-frequency peak may even disappear, see curve 2.

To exemplify how the photon-drag current may depend on the number of wells in the structure we have plotted in Fig. 12 the normalized drag current as a function of the incident photon energy for different numbers of wells, viz., 1 (curve 1), 2 (curve 2), 10 (curve 3), 40 (curve 4), 80 (curve 5), 150 (curve 6), and 200 (curve 7). In all cases the angle of incidence is $\theta=60°$, and the spatial period of the structure is $\Delta=400$ Å. Since the angle of incidence is rather large the spectra display one peak only, see curve 2 of Fig. 11. When the number of wells is small, the photon drag current increases proportional to the number of wells. This is so because the all-over radiative coupling is weak and the background field is the same on each well. In Fig. 12 this proportionality appears when the currents belonging to

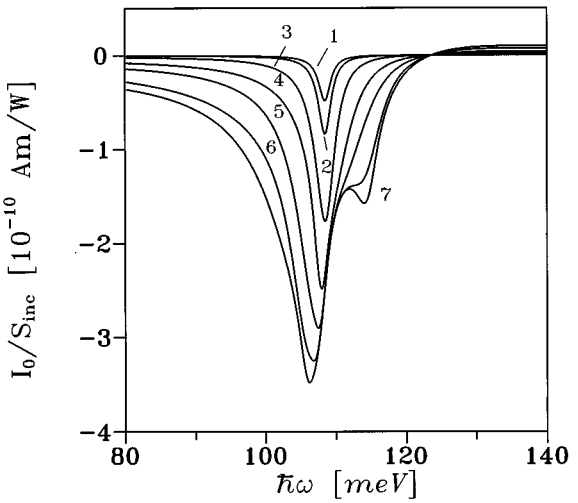

FIG. 12. Photon-drag current normalized by the magnitude of the incident Poynting vector as a function of incident photon energy for different numbers of wells, viz., 1 (curve 1), 2 (curve 2), 10 (curve 3), 40 (curve 4), 80 (curve 5), 150 (curve 6), and 200 (curve 7). In all cases the angle of incidence is $\theta=60°$ and the spatial period of the structure is $\Delta=400$ Å.

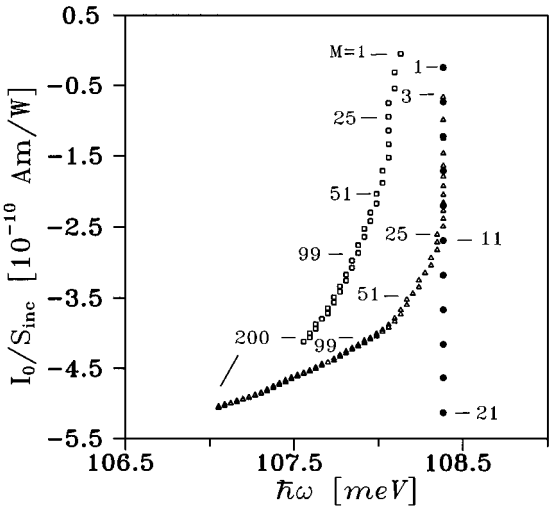

FIG. 13. Mutual values of the peak height of the normalized photon-drag current at resonance and its location in frequency shown for different numbers (M) of quantum wells. The spatial period of the structure is $\Delta=400$ Å and the angle of incidence is either $\theta=20°$ (□) or $\theta=60°$ (△). Results without inclusion of the radiative coupling among the wells are plotted in black circles (●) for $\theta=60°$.

curves 1 and 2 are compared. With an increase of the number of wells, more wells contribute to the radiative interaction process and this changes the internal dynamics of each well. As a result the rate of increase in the current with the well number becomes smaller. When the number of wells is increased up to $M\simeq150$ a shoulder appears on the high-frequency side of the peak, and for $M\simeq200$ this shoulder has developed into a peak.

When the number of wells is increased the peak in the photon-drag current increases and is shifted downwards in frequency, see Fig. 12. A systematic display of this aspect is shown in Fig. 13, where the current peak height and the associated resonance frequency have been shown for different numbers of quantum wells in the range $1\leqslant M\leqslant200$. The spatial period of the structure is as in Fig. 12, $\Delta=400$ Å. The angle of incidence is either $\theta=20°$ (□) or $\theta=60°$ (△). For comparison, results obtained without inclusion of the radiative coupling are shown by the black circles (●) for $\theta=60°$. If the radiative coupling among the wells is ignored the resonance peaks belonging to the various number of wells are located at the same frequency ($\omega=108.4$ meV). This frequency, which thus is the resonance frequency for just one well, is blueshifted with respect to the electronic resonance frequency $\varepsilon_{21}=99.7$ meV and this shift originates in local-field effects caused by the self-field dynamics. The self-field dynamics is described in the Green's function formalism by the delta-function part $[(c/\omega)^2\delta(z'-z)\mathbf{e}_z\mathbf{e}_z]$ of the propagator in Eq. (26).[12] As long as the number of wells is so small that the background field acting on each well is the same the photon-drag current increases proportional to the number of wells, as may be seen from the equidistance of the black circles. Now, when the radiative coupling among the wells is turned on (the triangular points for $\theta=60°$), the situation changes radically. Thus, for small well numbers ($M\lesssim25$) the rate of increase of the photon-drag peak is much less, although the peak stays at the same frequency as in the uncoupled calculation. When the number of wells is increased beyond, say, $M\simeq25$ the peak location tends to be shifted downwards in frequency, and as the structure contains more and more wells the rate of this downwards shift gradually becomes smaller and the current tends to saturate. For $M=200$ the resonance frequency is still far above the electronic transition frequency, however. Altogether it appears that self-field effects give a significant blueshift of the single-well resonance frequency with respect to the electronic resonance and when the radiative coupling among the wells is turned on the resonance frequency experiences a

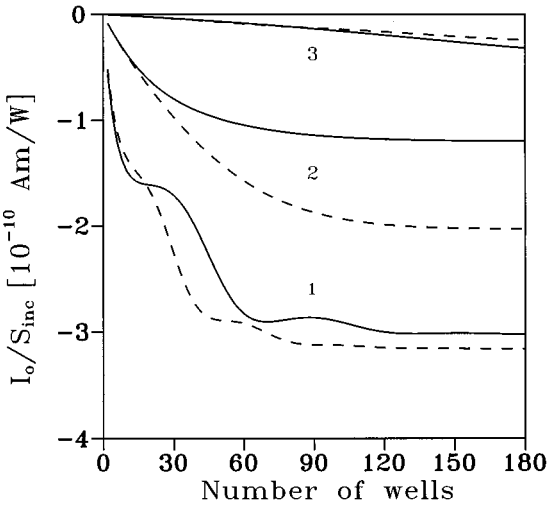

FIG. 14. Photon-drag current normalized by the magnitude of the incident Poynting vector as a function of the number of wells for three different photon energies, viz., 108 meV (curve 1), 112 meV (curve 2), and 120 meV (curve 3). The solid and dashed lines represent results for the spatial periods $\Delta=200$ and 400 Å, respectively. The angle of incidence is in both cases $\theta=60°$.

(smaller) redshift from the single-well resonance. When the angle of incidence is $\theta=20°$ the effects are qualitatively as discussed above, though the saturation tendency is no so pronounced for $M=200$.

In Fig. 14 is shown the normalized drag current as a function of the number of wells for three different incident photon energies, viz., 108 meV (curve 1), 112 meV (curve 2), and 120 meV (curve 3). The solid and dashed lines present results for the spatial periods $\Delta=200$ and 400 Å, respectively, and the angle of incidence is in all cases $\theta=60°$. It appears from Fig. 14 that, when the number of the wells is less than, say, 15, the increase of the drag current is proportional to the number of wells. As the number of wells is larger than $M\gtrsim 15$, and the incident energy is close to the resonance energy, as it is in curves 1 and 2, the radiative coupling among the wells becomes important, and the drag currents start to saturate, see Fig. 13. If the incident energy is far from resonance, the drag current continues to increase (curve 3) almost linearly with the well number. By changing the spatial period of the structure to 400 Å, the difference between the two results is small for $M\lesssim 15$. With increasing well numbers the radiative interaction processes become more significant.

In summary, in this paper we have derived general expressions for the photon-drag current along the quantum well. Then, limiting ourselves to two-level quantum-well systems, we have carried out numerical calculations of the photon-drag current in single and in multiple quantum-well structures as functions of the photon energy, angle of incidence, and number of wells. Special attention has been paid to the importance of the local-field corrections, as well as the radiative coupling among the wells. It appears that these corrections may have a substantial effect on the photon-drag current. In the present theory the blueshift and the asymmetric shape of the photon-drag current have been ascribed to local-field effects.

ACKNOWLEDGMENT

One of the authors (X.C) would like to thank the Daloon Foundation for the financial support which enabled him to carry out the present research.

APPENDIX: CALCULATION OF THE PHOTON-DRAG RESPONSE TENSORS

In this appendix we indicate how the integrations over the $\mathbf{k}_\parallel$ domain in Eq. (11) can be carried out in a convenient manner. From the components of the transition current density parallel to the plane of the quantum well it appears that one has to evaluate the vectorial quantity

$$\mathbf{R}^{(nm)}=\int_{-\infty}^{\infty}\frac{f_0[\varepsilon_n+\hbar^2|\mathbf{k}_\parallel-\mathbf{q}_\parallel|^2/(2m_0)]-f_0[\varepsilon_m+\hbar^2k_\parallel^2/(2m_0)]}{\hbar(\omega+i/\tau)+\varepsilon_n-\varepsilon_m+\hbar^2|\mathbf{k}_\parallel-\mathbf{q}_\parallel|^2/(2m_0)-\hbar^2k_\parallel^2/(2m_0)}\,(2\mathbf{k}_\parallel-\mathbf{q}_\parallel)\,\frac{d^2k_\parallel}{(2\pi)^2}. \tag{A1}$$

Written out in Cartesian coordinates the integrand is an uneven function of $k_{\parallel,y}$ and with the choice $\mathbf{q}_\parallel=q_\parallel\mathbf{e}_x$, Eq. (A1) is thus reduced to

$$\mathbf{R}^{(nm)}=(R_-^{(nm)}-R_+^{(nm)})\mathbf{e}_x, \tag{A2}$$

where

$$\begin{aligned}R_-^{(nm)}&=\int_{-\infty}^{\infty}\frac{f_0[\varepsilon_n+\hbar^2|\mathbf{k}_\parallel-\mathbf{q}_\parallel|^2/(2m_0)]}{\hbar(\omega+i/\tau)+\varepsilon_n-\varepsilon_m+\hbar^2|\mathbf{k}_\parallel-\mathbf{q}_\parallel|^2/(2m_0)-\hbar^2k_\parallel^2/(2m_0)}\,(2\mathbf{k}_\parallel\cdot\mathbf{e}_x-q_\parallel)\,\frac{d^2k_\parallel}{(2\pi)^2}\\&=\int_{-\infty}^{\infty}\frac{f_0[\varepsilon_n+\hbar^2k_\parallel^2/(2m_0)]}{\hbar(\omega+i/\tau)+\varepsilon_n-\varepsilon_m+\hbar^2k_\parallel^2/(2m_0)-\hbar^2|\mathbf{k}_\parallel+\mathbf{q}_\parallel|^2/(2m_0)}\,(2\mathbf{k}_\parallel\cdot\mathbf{e}_x+q_\parallel)\,\frac{d^2k_\parallel}{(2\pi)^2},\end{aligned} \tag{A3}$$

and

$$R_+^{(nm)}=\int_{-\infty}^{\infty}\frac{f_0[\varepsilon_m+\hbar^2k_\parallel^2/(2m_0)]}{\hbar(\omega+i/\tau)+\varepsilon_n-\varepsilon_m+\hbar^2|\mathbf{k}_\parallel-\mathbf{q}_\parallel|^2/(2m_0)-\hbar^2k_\parallel^2/(2m_0)}\,(2\mathbf{k}_\parallel\cdot\mathbf{e}_x-q_\parallel)\,\frac{d^2k_\parallel}{(2\pi)^2}. \tag{A4}$$

The component of the transition current density perpendicular to the well plane leads to the consideration of the quantity

$$H^{(nm)}=H_-^{(nm)}-H_+^{(nm)}, \tag{A5}$$

where

$$H_-^{(nm)}=\int_{-\infty}^{\infty}\frac{f_0[\varepsilon_n+\hbar^2k_\parallel^2/(2m_0)]}{\hbar(\omega+i/\tau)+\varepsilon_n-\varepsilon_m+\hbar^2k_\parallel^2/(2m_0)-\hbar^2|\mathbf{k}_\parallel+\mathbf{q}_\parallel|^2/(2m_0)}\,\frac{d^2k_\parallel}{(2\pi)^2}, \tag{A6}$$

$$H_+^{(nm)}=\int_{-\infty}^{\infty}\frac{f_0[\varepsilon_m+\hbar^2k_\parallel^2/(2m_0)]}{\hbar(\omega+i/\tau)+\varepsilon_n-\varepsilon_m+\hbar^2|\mathbf{k}_\parallel-\mathbf{q}_\parallel|^2/(2m_0)-\hbar^2k_\parallel^2/(2m_0)}\,\frac{d^2k_\parallel}{(2\pi)^2}. \tag{A7}$$

By using the low-temperature ($T=0$ K) approximation for the Fermi-Dirac distribution function, i.e., $f_0[\varepsilon_i+\hbar^2k_\parallel^2/(2m_0)]=\vartheta[E_F-\varepsilon_i-\hbar^2k_\parallel^2/(2m_0)]$, $i=m, n$, and by introducing polar coordinates $[k_{\parallel,x},k_{\parallel,y}]=k_\parallel[\cos\theta,\sin\theta]$, the four integrals in Eqs. (A1)–(A7) take the forms

$$R_+^{(nm)}=\int_0^{k_\parallel^{\max}}\int_0^{2\pi}\frac{(2k_\parallel\cos\theta-q_\parallel)k_\parallel}{\alpha_+^{(nm)}-\beta k_\parallel\cos\theta}\frac{d\theta dk_\parallel}{(2\pi)^2}\,\vartheta(E_F-\varepsilon_m), \tag{A8}$$

$$R_-^{(nm)}=\int_0^{k_\parallel^{\max}}\int_0^{2\pi}\frac{(2k_\parallel\cos\theta+q_\parallel)k_\parallel}{\alpha_-^{(nm)}-\beta k_\parallel\cos\theta}\frac{d\theta dk_\parallel}{(2\pi)^2}\,\vartheta(E_F-\varepsilon_n), \tag{A9}$$

and

$$H_+^{(nm)}=\int_0^{k_\parallel^{\max}}\int_0^{2\pi}\frac{k_\parallel}{\alpha_+^{(nm)}-\beta k_\parallel\cos\theta}\frac{d\theta dk_\parallel}{(2\pi)^2}\,\vartheta(E_F-\varepsilon_m), \tag{A10}$$

$$H_-^{(nm)}=\int_0^{k_\parallel^{\max}}\int_0^{2\pi}\frac{k_\parallel}{\alpha_-^{(nm)}-\beta k_\parallel\cos\theta}\frac{d\theta dk_\parallel}{(2\pi)^2}\,\vartheta(E_F-\varepsilon_n), \tag{A11}$$

where $\alpha_\pm^{(nm)}$ and β are given in Eqs. (19) and (21) and $k_\parallel^{\max}=[2m_0(E_F-\varepsilon_i)]^{1/2}/\hbar$. Performing, finally, the integrals over θ and $k_\parallel$ one obtains the results in Eqs. (17) and (18).

[1] S. Luryi, Phys. Rev. Lett. **58**, 2263 (1987).
[2] A. A. Grinberg and S. Luryi, Phys. Rev. B **38**, 87 (1988).
[3] M. I. Stockman, L. N. Pandey, and T. F. George, Phys. Rev. Lett. **65**, 3433 (1990).
[4] O. Keller, Phys. Rev. B **48**, 4786 (1993).
[5] F. T. Vasko, Phys. Rev. B **53**, 9576 (1996).
[6] A. D. Wieck, H. Sigg, and K. Ploog, Phys. Rev. Lett. **64**, 463 (1990).
[7] R. Kesselring, A. W. Kalin, H. Sigg, and F. Kneubuhl, Rev. Sci. Instrum. **63**, 3317 (1992).
[8] V. M. Shalaev, C. Douketis, and M. Moskovits, Phys. Lett. A **169**, 205 (1992).
[9] V. M. Shalaev, C. Douketis, J. T. Stuckless, and M. Moskovits, Phys. Rev. B **53**, 11 388 (1996).
[10] O. Keller, in *Studies in Classical and Quantum Nonlinear Optics*, edited by O. Keller (Nova Science, New York, 1995), p. 269.
[11] O. Keller and A. Liu, Phys. Scr. **51**, 531 (1995).
[12] O. Keller, Phys. Rep. **268**, 85 (1996).
[13] E. V. Alieva, E. I. Firsov, L. A. Kuzik, V. A. Yakovlev, and F. A. Pudonin, Phys. Lett. A **152**, 89 (1991).